Journal of Alloys and Compounds 506 (2010) 216–223

Contents lists available at ScienceDirect

Journal of Alloys and Compounds

journal homepage: www.elsevier.com/locate/jallcom

The influence of addition of Al nano-particles on the microstructure and shear strength of eutectic Sn–Ag–Cu solder on Au/Ni metallized Cu pads

Asit Kumar Gain[a], Tama Fouzder[a], Y.C. Chan[a,*], A. Sharif[b], N.B. Wong[c], Winco K.C. Yung[d]

[a] Department of Electronic Engineering, City University of Hong Kong, Tat Chee Avenue, Kowloon Tong, Hong Kong
[b] Department of Materials and Metallurgical Engineering, Bangladesh University of Engineering and Technology, Dhaka 1000, Bangladesh
[c] Department of Biology and Chemistry, City University of Hong Kong, Tat Chee Avenue, Kowloon Tong, Hong Kong
[d] Department of Industrial and Systems Engineering, The Hong Kong Polytechnic University, Hung Hom, Kowloon, Hong Kong

ARTICLE INFO

Article history:
Received 31 March 2010
Received in revised form 28 June 2010
Accepted 30 June 2010
Available online 7 July 2010

Keywords:
Nano-doping
Ball grid array solder joints
Shearing force
Microstructure

ABSTRACT

In order to identify the effect of the addition of Al nano-particles to eutectic Sn–Ag–Cu solder, the interfacial microstructure between the solder and Au/Ni metallized Cu pad ball grid array substrates has been investigated as a function of multiple reflow cycles as well as aging time. Also the strength of the solder joints was evaluated by a ball shear test. In Sn–Ag–Cu solder joints and solder joints containing Al nano-particles, a scallop-shaped Sn–Ni–Cu intermetallic compound layer was clearly observed at the interfaces after long time aging and multiple reflows, and the intermetallic compound layer thickness was substantially increased with an increase in the number of reflow cycles as well as the aging time. However, after the addition of Al nano-particles, an additional Sn–Al–Ag intermetallic compound was found on the top surface of the Sn–Ni–Cu intermetallic compound layer. The Sn–Ag–Cu solder joints containing 3 wt% Al nano-particles consistently displayed a higher shear strength than that of the plain Sn–Ag–Cu solder joints as well as a lower Al nano-particle content as a function of reflow cycles and aging time due to a second phase dispersion strengthening mechanism by the formation of fine Sn–Ag–Al intermetallic compound particles as well as a controlled fine microstructure.

1. Introduction

Environmental and health concerns, public sentiment and market strategies as well as government regulations and legislation have been the driving force to eliminate the applications of toxic lead and lead-containing compounds in microelectronic devices [1–3]. Therefore, rapid switching to lead-free solders has occurred to replace lead-based solders in the packaging process of electronic devices and components. In fact, many research groups have been focused on developing new lead-free solders. But new solders must fulfill several requirements such as wettability, a suitable melting temperature, good mechanical properties, good resistance to mechanical and thermal fatigue, corrosion resistance, good electrical properties, acceptable for health and the environment, availability and low material cost [4,5]. Up to now, several types of binary and ternary Sn-based lead-free solders such as Sn–Zn, Sn–Ag, Sn–Cu, Sn–Ag–Zn and Sn–Ag–Cu have been developed and applied in the electronic packaging industry [6–8]. Among them, Sn–Ag–Cu solder has been proposed as one of the most promising substitutes for lead-containing solder because of its good basket of properties, such as superior solderability as well as good compatibility with current components and processing routes [9–11].

Moreover, with the advancement of micro-/nanosystem technologies through the years, microelectronic components have evolved to become smaller, lighter and more functional. Therefore, conventional solder technology can no longer guarantee the solder joint reliability for electronic components [12]. In general, the reliability of solder joints is mainly dependent on wettability between the molten solder/substrate, the coefficients of thermal expansion of the components of the joints, their yield strength, shear strength, elastic modulus, fatigue and creep behavior [13,14]. A viable approach to improve the performance of a solder joint in terms of electrical, thermal and mechanical properties is to add appropriate second phase particles, of a ceramic, metallic or intermetallic, to a solder matrix so as to form a composite [15,16]. In the existing literature, micro-/nanometer sized particles of alloying elements such as silver, copper, nickel, antimony and bismuth improved the mechanical properties of a lead-free solder while simultaneously reducing the melting point [17,18]. In addition, various nano-sized, nonreacting, noncoarsening oxide dispersoids have been incorporated into solder alloys to create a new, improved solder structure which exhibits significantly enhanced creep resistance combined with increased strength [19]. Tai et al. [20] prepared 20 vol.% Cu_6Sn_5 reinforced Sn–3.5Ag com-

* Corresponding author. Tel.: +852 27887130; fax: +852 27887579.
E-mail address: eeycchan@cityu.edu.hk (Y.C. Chan).

0925-8388/$ – see front matter © 2010 Elsevier B.V. All rights reserved.
doi:10.1016/j.jallcom.2010.06.180

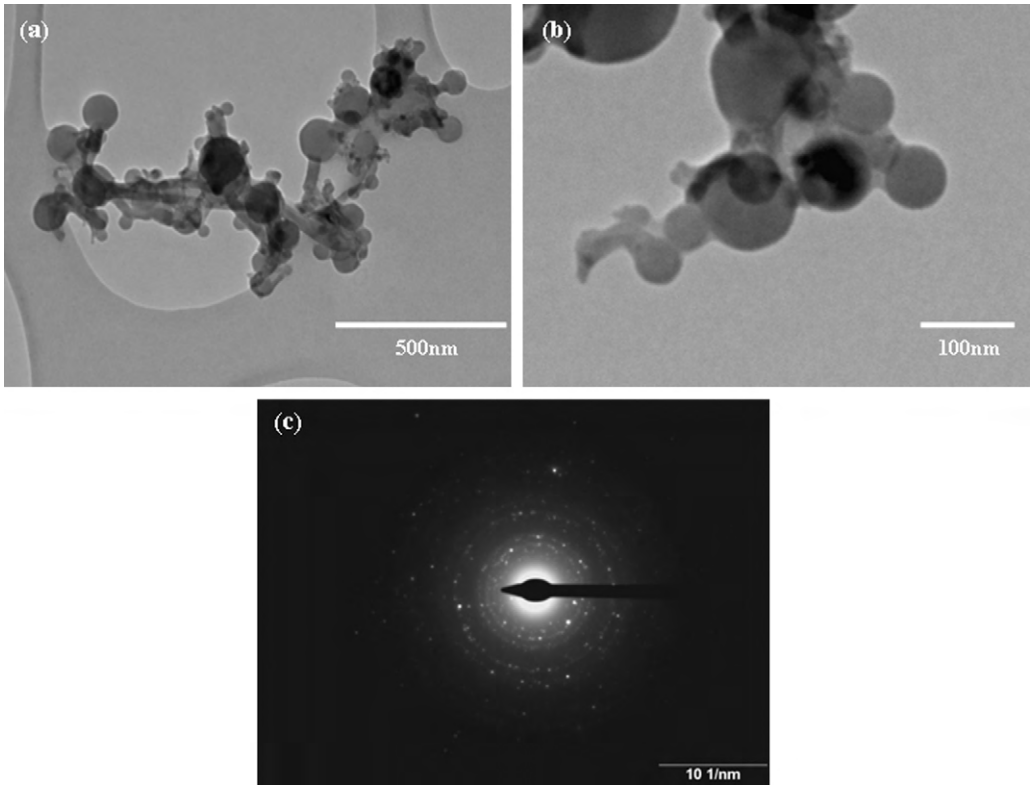

Fig. 1. Bright field TEM images of (a and b) Al nano-particles and (c) a selected area diffraction pattern of the Al nano-particles.

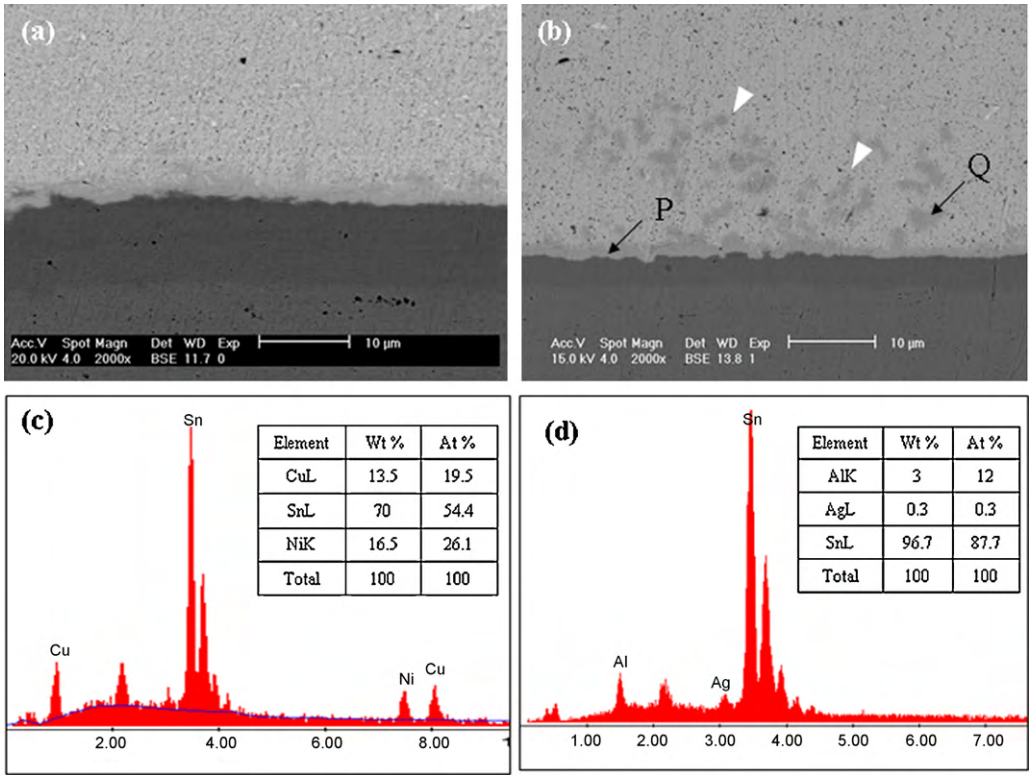

Fig. 2. SEM micrographs of (a) a Sn–Ag–Cu solder joint and (b) a Sn–Ag–Cu solder joint containing 3 wt% Al nano-particles after one reflow cycle, (c) and (d) EDS and elemental analysis of regions marked P and Q in (b).

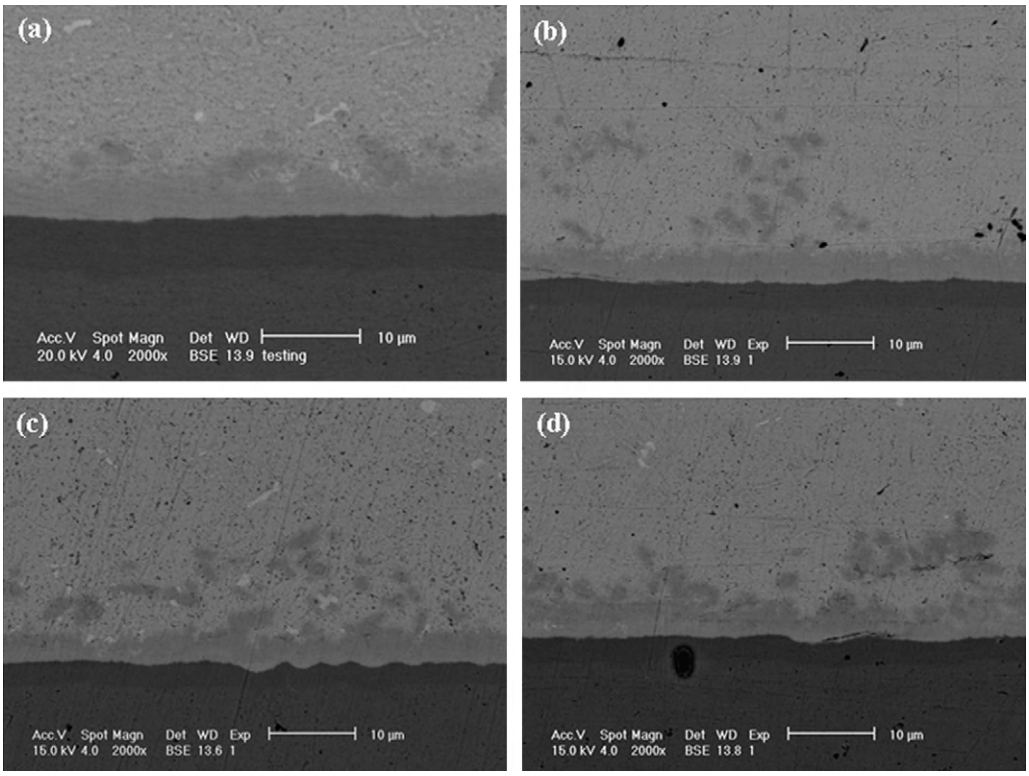

Fig. 3. SEM micrographs of Sn–Ag–Cu solder joints after eight reflow cycles with Al nano-particle contents: (a) 0 wt%, (b) 0.5 wt%, (c) 1 wt% and (d) 3 wt%.

posite solder by an in situ method and the composite solder joint exhibited better steady-state creep strain rate, less thermomechanical fatigue damage and higher shear strengths after different numbers of thermomechanical fatigue cycles as compared to a plain Sn–3.5Ag solder joint. Xiao et al. [21] reported that rare earth (Ce, La) reinforced Sn–Ag–Cu composite solders suppressed the formation of intermetallic compounds and refined the microstructure. In addition, the creep-rupture lifetime of the rare earth doped Sn–Ag–Cu solder joint was significantly improved being seven times higher than that of undoped solder joints. Shen and Chan

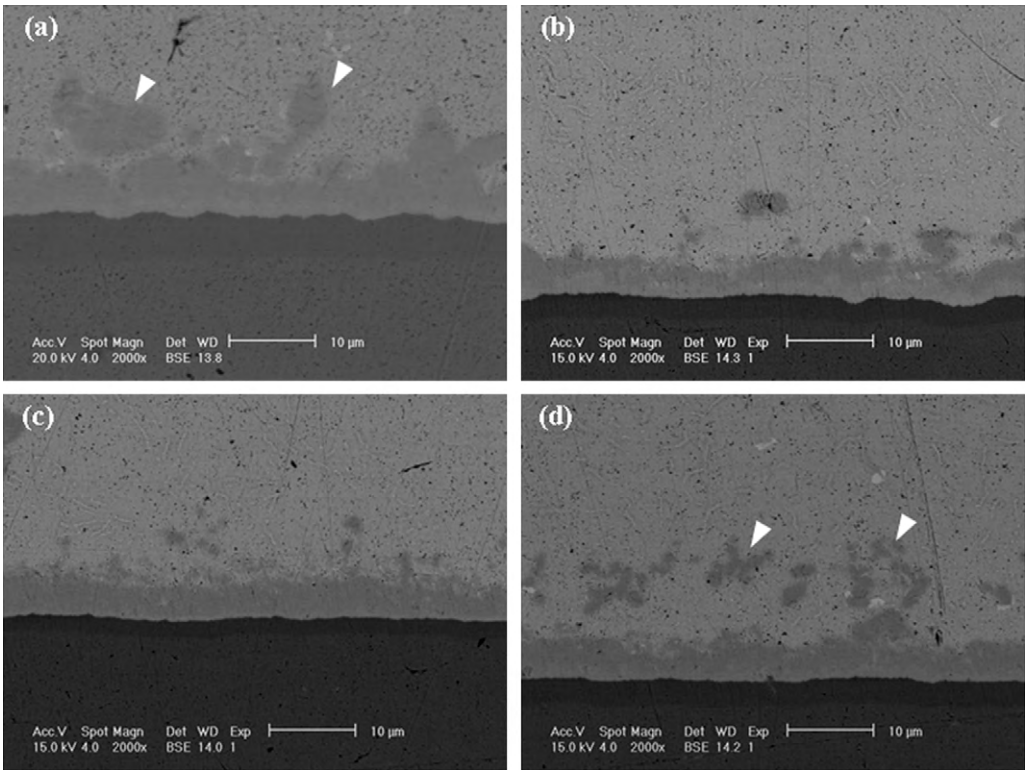

Fig. 4. SEM micrographs of Sn–Ag–Cu solder joints after 16 reflow cycles with Al nano-particle contents: (a) 0 wt%, (b) 0.5 wt%, (c) 1 wt% and (d) 3 wt%.

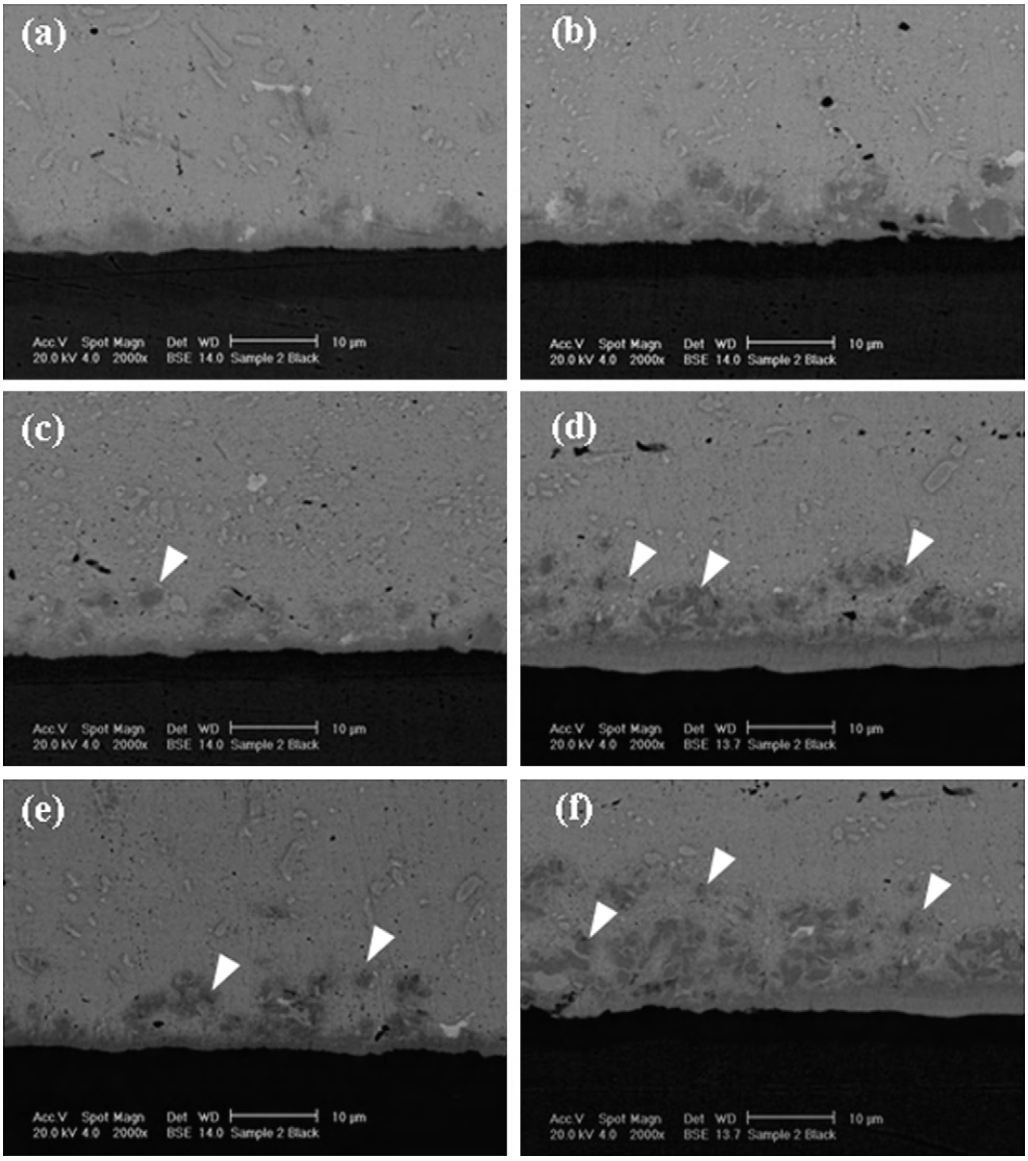

Fig. 5. SEM micrographs of (a) Sn–Ag–Cu, (c) Sn–Ag–Cu–1 wt%Al and (e) Sn–Ag–Cu–3 wt%Al solder joints after 10 days and (b) Sn–Ag–Cu, (d) Sn–Ag–Cu–1 wt%Al and (f) Sn–Ag–Cu–3 wt%Al solder joints after 40 days aging.

[22] successfully prepared a ZrO_2 reinforced composite solder by mechanically dispersing ZrO_2 nano-particles into a eutectic Sn–9Zn solder paste and this composite solder had a much improved the shear strength. Tsao and Chang [23] found that a Sn–3.8Ag–0.7Cu composite solder reinforced with TiO_2 nano-particles had a significantly improved hardness, yield strength and ultimate tensile strength.

However, the result of a literature search revealed that no studies have been reported so far on lead-free Sn–Ag–Cu solder joints containing Al nano-particles. Accordingly, the present study is focused on the solderability and interfacial microstructure of a eutectic Sn–Ag–Cu based solder reinforced with Al nano-particles on Au/Ni metallized Cu pads on ball grid array (BGA) substrates in an attempt to add to the knowledge base of lead-free composite solders. In addition, the shear strengths of plain Sn–Ag–Cu solder joints and solder joints containing Al nano-particles were measured on Au/Ni metallized Cu pads on ball grid array (BGA) substrates as a function of the number of reflow cycles as well as the aging time and with the content of Al nano-particles.

2. Experimental procedure

Composite solders were prepared by mechanically dispersing Al nano-particles (0, 0.5, 1 and 3 wt%) into a eutectic Sn–3.5Ag–0.5Cu (Showa Denko JUFFIT-E 9ZSN10M) solder powder. The mixture was blended manually for at least 30 min to achieve a uniform distribution of Al nano-particles with a water-soluble flux (Qualitek Singapore (PTE) Ltd.). Then, the paste mixture was printed on to alumina substrates using a stainless steel stencil with a thickness of 0.15 mm and reflowed in a reflow oven (BTU VIP-70N) at 250 °C to prepare approximately 760 μm diameter solder balls.

A solder mask-defined copper bond pad on the flexible substrate of a BGA package was used as a base for electrodeposition of Ni and Au. The solder mask-opening diameter was 0.6 mm and a 7 μm thick Ni layer was deposited in these openings. The average thickness of the Au layer was 0.5 μm. Lead-free solder balls with a diameter of 760 μm, were placed on the prefluxed Au/Ni/Cu bond pads of the substrates and reflowed at a temperature of 250 °C with a belt speed 71 cm/min in a convection reflow oven (BTU VIP-70N). After the reflow process, the samples were cooled to room temperature. Then, each BGA solder joint was cleaned with isopropyl alcohol (IPA). The assembled packages were then aged isothermally at 150 °C for 10–40 days in a high temperature oven to examine the interfacial reactions between the solder and the UBM. Finally, the as-reflowed and aged specimens were mounted in resin, then mechanically ground by different grit size emery papers and polished with an 0.5 μm Al_2O_3 suspension. A scanning electron microscope (SEM, Philips XL 40

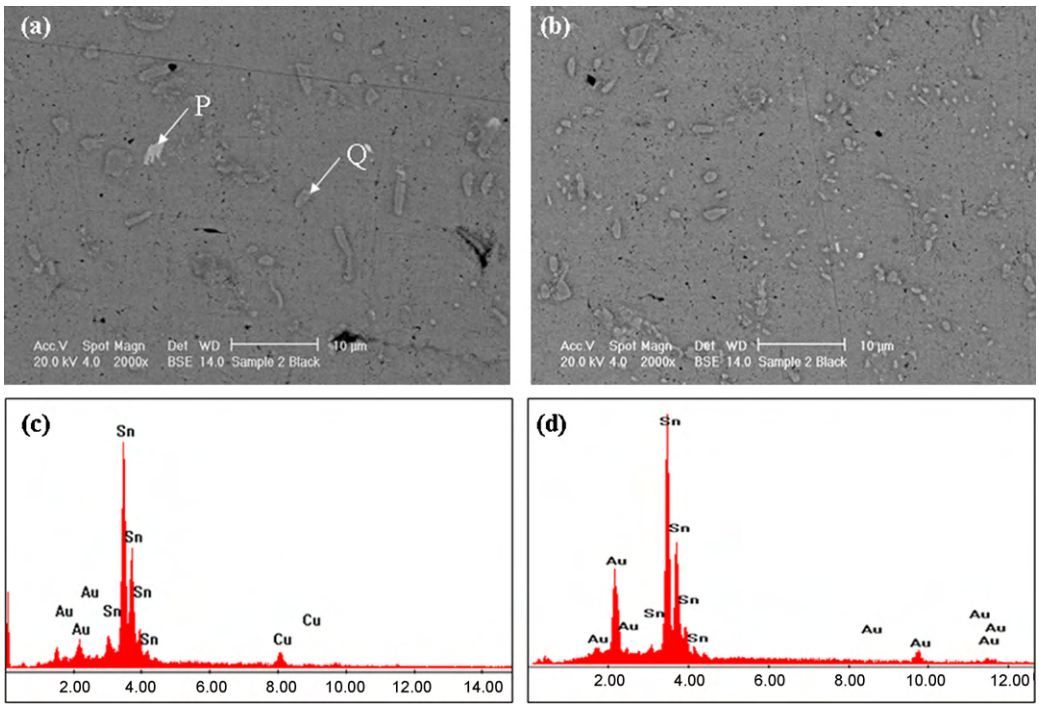

Fig. 6. SEM micrographs of (a) a Sn–Ag–Cu solder joint and (b) a Sn–Ag–Cu solder joint containing 3 wt% Al nano-particles after 40 days aging, (c) and (d) EDS and elemental analysis of regions marked P and Q in (a).

FEG) with the backscattered electron (BSE) imaging mode was used for the observation of the microstructures. Additionally, an energy dispersive X-ray spectrometer (EDX) (EDAX International, model no. DX-4) was adopted to determine phase compositions. The accuracy of the compositional measurements was typically ±5%. To find out the formula composition of the intermetallic compound (IMC) particles, the chemical analyses of the EDX spectra were corrected by standard atomic number, absorption, fluorescence (ZAF) software. Before the SEM observations, the samples were sputter coated with Au to avoid any effects due to charging. Transmission electron microscopy (TEM, CM 20, Philips) was used for the observation of the Al nano-particles.

To measure the shear strength, ball shear tests were performed on the reflowed and aged samples using a shear testing machine (PTR-1000, Rhesca Co. Ltd., Japan) with a 50 μm shear tool height and 550 μm/s shear speed. The average strength of 20 solder balls with the minimum and maximum values removed was taken for each condition. After ball shear testing, the fracture surfaces and compositions were investigated thoroughly using SEM and EDX techniques.

3. Results and discussion

Fig. 1(a and b) shows bright field TEM images of Al nano-particles and (c) a selected area diffraction pattern of Al nano-particles. In the TEM images, spherically-shaped Al nano-particles, about 80–100 nm, in diameter are clearly observed. In the low magnification TEM observation [Fig. 1(a)], it seems the nano-particles inside one cluster are in contact. However, when the sample was tilted and observed at a higher magnification, there was often some spaces between the particles as shown in Fig. 1(b).

The backscattered electron imaging mode of the SEM was utilized to help identify distinguishable interfacial phases between plain Sn–Ag–Cu or solder joints containing Al nano-particles and the Au/Ni metallized Cu pads on ball grid array (BGA) substrates. Fig. 2 shows backscattered scanning electron micrographs of (a) a plain Sn–Ag–Cu solder joints and (b) a Sn–Ag–Cu solder joint containing 3 wt% Al nano-particles after one reflow cycle at 250 °C. At their interfaces, a scallop-shaped Sn–Ni–Cu intermetallic compound layer with a dark contrast was clearly observed in both plain Sn–Ag–Cu solder and Sn–Ag–Cu solder joints containing 3 wt% Al nano-particles. However, after the addition of Al nano-particles at the interfaces of solder joints very fine dark contrast intermetallic compound particles were clearly observed as indicated with arrow heads in Fig. 2(b). During the initial reflow, the topmost thin (~0.5 μm) Au layer in the Au/Ni metallized Cu pads dissolved into the molten solder, leaving the Ni layer exposed to the plain molten Sn–Ag–Cu solder and solder joints containing Al nano-particles. Therefore, a scallop-shaped ternary Sn–Ni–Cu intermetallic compound layer appeared at their interfaces. EDS profiles (c) and (d) were taken from regions marked 'P' and 'Q' in Fig. 2(b). According to the EDS analysis, the composition of the ternary intermetalic compound layer marked 'P' consisted of a 54.4 at.% Sn, 26.1 at.% Ni and 19.5 at.% Cu phase. Yoon et al. [24] noted that there is a small atomic size difference between Cu and Ni, and since both have the same FCC lattice structure, the substitution of Ni into Cu_6Sn_5, without causing a lattice distortion or the formation of a new phase, was reasonable. According to the EDS analysis, the intermetalic compound particles marked 'Q' consisted of 87.7 at.% Sn, 12.0 at.% Al and 0.3 at.% Ag phase. From the EDS profile and elemental analysis in Fig. 2(d) it is clear that the dark contrast very fine intermetallic compound particles were a ternary Sn–Al–Ag phase.

Fig. 3 shows backscattered scanning electron micrographs of Sn–Ag–Cu solder joints with different weight percentages of Al nano-particles (a) 0 wt%, (b) 0.5 wt%, (c) 1 wt% and (d) 3 wt% after eight reflow cycles at 250 °C. A scallop-shaped ternary Sn–Ni–Cu intermetallic compound layer appeared at their interfaces in both plain Sn–Ag–Cu and solder joints containing Al nano-particles, the same as after one reflow cycle. In addition, Ag_3Sn, Cu_6Sn_5 and Au–Sn intermetallic compounds were clearly observed in the β-Sn matrix in both samples. Yoon and Jung [25] reported that the dissolved Ag and Cu were precipitated by forming Ag_3Sn and Cu_6Sn_5 intermetallic compounds in the solder matrix during solidification. In the solder ball region a Au–Sn intermetallic compound formed due to the diffusion of Au atoms from the Au/Ni metallized Cu pads. However, after the addition of Al nano-particles, additional fine ternary intermetallic Sn–Al–Ag compound particles were clearly observed on the top surface of the scallop-shaped ternary Sn–Ni–Cu intermetallic compound layer. In addition, as expected, the amount of fine ternary intermetallic Sn–Al–Ag compound par-

ticles increased with an increase in the weight percentage of Al nano-particles in the Sn–Ag–Cu solder as shown in Fig. 3(b–d).

Fig. 4 shows backscattered scanning electron micrographs of (a) plain Sn–Ag–Cu solder and solder joints with different weight percentages of Al nano-particles of (b) 0.5 wt%, (c) 1 wt% and (d) 3 wt% after 16 reflow cycles at 250 °C. After 16 reflow cycles, at their interfaces, scallop-shaped ternary Sn–Ni–Cu intermetallic compound layers with a dark contrast were clearly observed in both plain Sn–Ag–Cu solder joints and Sn–Ag–Cu solder joints containing Al nano-particles, the same as after one and eight reflow cycles. From Figs. 2–4, it was confirmed that the intermetallic compound layer thickness was substantially increased and appeared with a denser structure after an extended number of reflow cycles. In addition, in plain Sn–Ag–Cu solder joints spherically-shaped large size Sn–Ni–Cu intermetallic compound particles were also observed at the top surface of the intermetallic compound layer. However, after 16 reflow cycles in Sn–Ag–Cu solder joints containing 3 wt% Al nano-particles, some "sunflower" shaped ternary Sn–Al–Ag intermetallic compound particles were clearly observed as indicated with arrowheads in Fig. 4(d) at the top surface of the Sn–Ni–Cu intermetallic compound layer due to the heterogeneous nucleation containing Al and Sn.

Fig. 5 shows backscattered scanning electron micrographs of (a) Sn–Ag–Cu, (c) Sn–Ag–Cu–1 wt%Al and (e) Sn–Ag–Cu–3 wt%Al solder joints after 10 days aging and (b) Sn–Ag–Cu, (d) Sn–Ag–Cu–1 wt%Al and (f) Sn–Ag–Cu–3 wt%Al solder joints after 40 days aging. It is clear that the Sn–Ni–Cu intermetallic compound layer thickness increased substantially with an increase in the aging time in Sn–Ag–Cu solder joints and solder joints containing Al nano-particles as shown in Fig. 5. However, with the addition of Al nano-particles at the top surface of the intermetallic compound layer very fine Sn–Al–Ag intermetallic compound particles were clearly observed as indicated with arrowheads in Fig. 5(c–f) and the amount of Sn–Al–Ag intermetallic compound particles also increased with the addition of more Al nano-particles.

Fig. 6 shows backscattered scanning electron micrographs of (a) a plain Sn–Ag–Cu solder joint and (b) a solder joint containing 3 wt% Al nano-particles after 40 days aging at 150 °C which were taken from the solder ball region. Ag_3Sn and Cu_6Sn_5 as well as Sn–Au intermetallic compounds were clearly observed in the β-Sn matrix in both plain Sn–Ag–Cu solder joints and solder joints containing 3 wt% Al nano-particles. However, after the addition of Al nano-particles, the size of the Ag_3Sn and Cu_6Sn_5 as well as Sn–Au intermetallic compounds was remarkably decreased to become much finer particles as shown in Fig. 6(b). A plausible explanation here for the finer intermetallic compound particles is that they are heterogeneously nucleated during the formation of the Sn–Al–Ag intermetallic compound at the top surface of the Sn–Ni–Cu intermetallic compound layer as shown in Fig. 5(f).

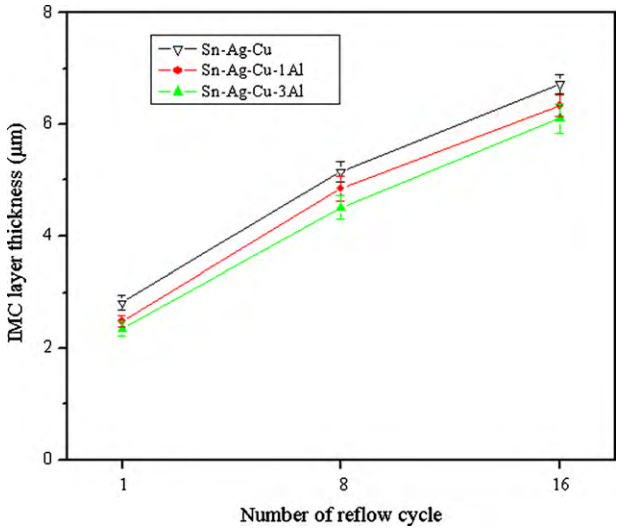

Fig. 7. IMC layer thickness of Sn–Ag–Cu–xAl composite solder joints as a function of the number of reflow cycles.

During the reflow process, the molten solders react with substrates resulting in the formation of intermetallic compounds (IMCs) at the interface. It is well known that intermetallic compounds (IMCs) at the interface have a significant effect on the performance of joints. Therefore, information on interfacial reactions between the solder and substrate as well as the intermetallic compound (IMC) layer thicknesses are fundamentally important for an evaluation of the reliability of solder joints. Fig. 7 shows the change of intermetallic compound layer thickness of plain Sn–Ag–Cu and solder joints containing Al nano-particles as a function of the number of reflow cycles. The IMC layer thicknesses of plain Sn–Ag–Cu solder joints and Sn–Ag–Cu solder joints containing 3 wt% Al nano-particles after one reflow cycle were about 2.8 and 2.4 μm, respectively and their IMC layer thicknesses after 16 reflow cycles were about 6.7 and 6.1 μm, respectively. From this result, it is confirmed that the Al nano-particles retarded the growth of the intermetallic compound layer.

Since solder joints are often subjected to mechanical loading during processing and system use, the mechanical properties of solder joints, such as shear strength is crucial to their reliability. Therefore, ball shear tests were performed to evaluate the effect of the interfacial reactions on the mechanical reliability of

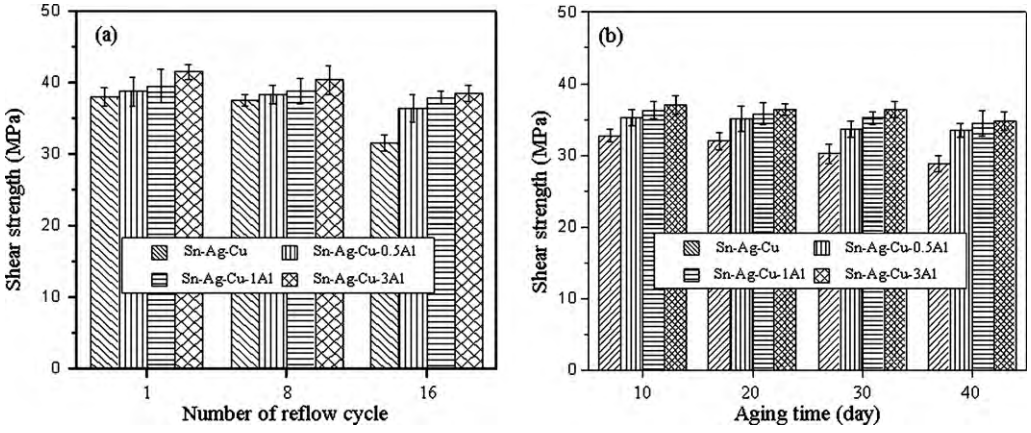

Fig. 8. Shear strength of Sn–Ag–Cu–Al composite solder joints as a (a) function of the number of reflow cycles and (b) aging time.

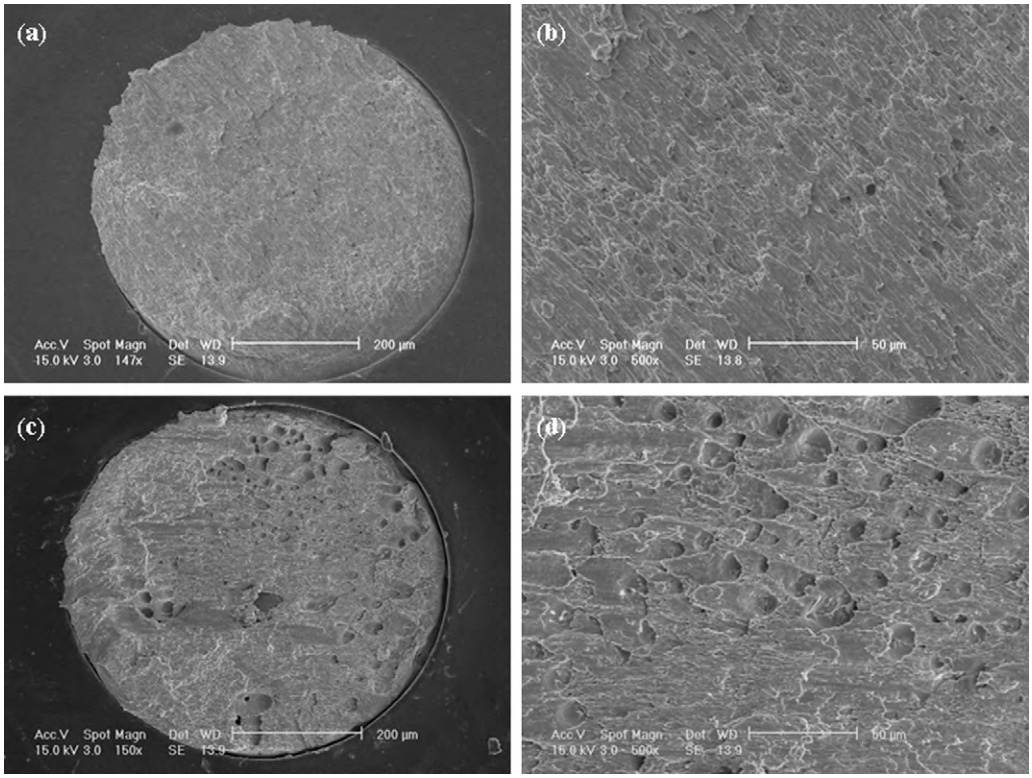

Fig. 9. SEM fracture surfaces of (a and b) Sn–Ag–Cu solder joints and (c and d) solder joints containing 3 wt% Al nano-particles after one reflow cycle.

Sn–Ag–Cu–*x*Al solder joints on Au/Ni metallized Cu pad BGA substrates as a function of the number of reflow cycles and aging time. Fig. 8 shows the variation of ball shear strength of plain Sn–Ag–Cu and Sn–Ag–Cu solder joints containing Al nano-particles as a function of the number of reflow cycles (a) and aging time (b). The shear strength of plain Sn–Ag–Cu solder joints after one reflow cycle was about 38 MPa while the shear strength after 16 reflow cycles was about 31.6 MPa. On the whole, the shear strength of solder joints containing Al nano-particles changed very little as a function of the number of reflow cycles due to the formation of the fine Sn–Ag–Al intermetallic compound particles and the refined Cu_6Sn_5, Ag_3Sn and Au–Sn intermetallic compound particles. However, the Sn–Ag–Cu–3 wt%Al solder joints consistently display a higher shear strength than that of the plain Sn–Ag–Cu solder joints as well as the lower Al nano-particle content joints for each reflow cycle and aging time. The higher shear strength of the Al nano-particles doped solder joints may be attributed to the formation of the fine Cu_6Sn_5, Ag_3Sn and Au–Sn IMCs that are dispersed throughout the β-Sn matrix at the top surface of the Sn–Ni–Cu intermetallic compound layers. The presence of such fine particles can act as obstacles for the movement of dislocations and subsequently strengthening due the dispersion of these particles [26] can be considered as a plausible explanation for the higher strength in nano-doped solder joints compared with that of the undoped joints. The shear strengths of solder joints containing 0.5 and 3 wt% Al nano-particles after one reflow cycle were about 38.8 and 41.5 MPa, respectively and their shear strengths after 16 reflow cycles were about 36.4 and 38.5 MPa, respectively. On the other hand, after aging at 150 °C for 40 days, the shear strength of plain Sn–Ag–Cu solder joints and solder joints containing 3 wt% Al nano-particles were about 28.8 and 34.8 MPa, respectively. After aging at high a temperature (150 °C) for 40 days the shear strength of solder joints containing Al nano-particles did not change significantly due to the formation of Sn–Al–Ag intermetallic compound particles as well as the refined microstructure in the solder matrix. For the Al nano-particles doped solder, fracture occurred through the bulk of the solder and the strength of the solder joint thus depends on that of the bulk solder. Due to a second phase dispersion strengthening mechanism, the solder retained its high strength even after multiple reflows as well as after a long time aging.

In order to compare the effect of the addition of Al nano-particles to Sn–Ag–Cu solder joints on Au/Ni metallized Cu pad BGA substrates the fracture surfaces were examined after ball shear tests. Fig. 9 shows SEM micrographs of the fracture surfaces of (a and b) plain Sn–Ag–Cu solder joints and (c and d) Sn–Ag–Cu solder joints containing 3 wt% Al nano-particles. The fracture surface of plain Sn–Ag–Cu solder joints exhibited a brittle fracture mode with a smooth surface as shown in Fig. 9(a and b). On the other hand, Sn–Ag–Cu solder joints containing Al nano-particles showed ductile failure with very rough dimpled fracture surfaces as shown in Fig. 9(c and d) due to the formation of the fine Sn–Al–Ag intermetallic compound particles.

4. Conclusions

Small amounts of Al nano-particles were added into the Sn–Ag–Cu solder alloy to investigate the effect of the addition of Al nano-particles on the formation, growth and evolution of the intermetallic compound layer structure at Au/Ni metalized Cu pad BGA substrates/solder interfaces. After multiple reflows and long time aging, a Sn–Ni–Cu intermetallic compound layer was formed at their interfaces in both plain Sn–Ag–Cu solder joints and solder joints containing Al nano-particles. The intermetallic compound layer thickness was substantially increased with an increase in the number of reflow cycles as well as aging time. During the reflow process Au atoms diffused and formed Au–Sn, Ag_3Sn and Cu_6Sn_5 intermetallic compounds which were clearly observed in the β-Sn matrix in both types of solder joints. However, after the addition of Al nano-particles, very fine ternary Sn–Al–Ag intermetallic compound particles were found at the top surface of the

Sn–Ni–Cu intermetallic compound layers as well as a more refined microstructure.

The solder joints with a high percentage of Al nano-particles showed a consistently higher strength than that of solder joints with a lower content of Al nano-particles at all numbers of reflow cycles as well as a function of aging time. It is reasonable to suggest that the strength of the bulk solder was enhanced by the formation of fine Sn–Al–Ag intermetallic particles as well as the controlled fine microstructure after long time aging. The failure mode of Sn–Ag–Cu solder joints containing Al nano-particles appeared to be ductile fracture with very rough dimpled surfaces due to the formation of fine Sn–Al–Ag intermetallic compound particles at the top surface of Sn–Ni–Cu intermetallic compound layer.

Acknowledgements

The authors acknowledge the financial support provided by City University of Hong Kong for the project 9041222 CERG grant of Hong Kong Research Grants Council and RGC ref. no. 111307 (Development of a nano-activator doped surface modifier for Sn–Zn based lead-free soldering). Professor Brian Ralph is thanked for proof reading the manuscript.

References

[1] L. Liu, W. Zhou, B. Li, P. Wu, J. Alloys Compd. 482 (2009) 90–98.
[2] H. Tsukamoto, T. Nishimura, S. Suenaga, K. Nogita, Mater. Sci. Eng. B 171 (2010) 162–171.
[3] A.K. Gain, Y.C. Chan, W.K.C. Yung, Mater. Sci. Eng. B 162 (2009) 92–98.
[4] J. Wan, Y. Liu, C. Wei, Z. Gao, J. Alloys Compd. 463 (2008) 230–237.
[5] K. Kanlayasiri, M. Mongkolwongrojn, T. Ariga, J. Alloys Compd. 485 (2009) 225–230.
[6] C.Y. Lin, U.S. Mohanty, J.H. Chou, J. Alloys Compd. 501 (2010) 204–210.
[7] A.K. Gain, Y.C. Chan, A. Sharif, W.K.C. Yung, Microelectron. Eng. 86 (2009) 2347–2353.
[8] W. Chen, S. Xue, H. Wang, Mater. Des. 31 (2010) 2196–2200.
[9] H.B. Kang, J.H. Bae, J.W. Lee, M.H. Park, Y.C. Lee, J.W. Yoon, S.B. Jung, C.W. Yang, Scr. Mater. 60 (2009) 257–260.
[10] Y.W. Wang, Y.W. Lin, C.T. Tu, C.R. Kao, J. Alloys Compd. 478 (2009) 121–127.
[11] J.X. Wang, S.B. Xue, Z.J. Han, S.L. Yu, Y. Chen, Y.P. Shi, H. Wang, J. Alloys Compd. 467 (2009) 219–226.
[12] P. Babaghorbani, S.M.L. Nai, M. Gupta, J. Alloys Compd. 478 (2009) 458–461.
[13] Z.X. Li, M. Gupta, Adv. Eng. Mater. 7 (11) (2005) 1049–1054.
[14] J. Shen, Y.C. Chan, J. Alloys Compd. 477 (2009) 909–914.
[15] P. Yao, P. Liu, J. Liu, Microelectron. Eng. 86 (2009) 1969–1974.
[16] J. Shen, Y.C. Chan, Microelectron. Reliab. 49 (2009) 223–234.
[17] P. Yao, P. Liu, J. Liu, J. Alloys Compd. 462 (2008) 73–79.
[18] A.K. Gain, Y.C. Chan, A. Sharif, N.B. Wong, W.K.C. Yung, Microelectron. Reliab. 49 (2009) 746–753.
[19] P. Babaghorbani, S.M.L. Nai, M. Gupta, J. Mater. Sci.: Mater. Electron. 20 (2009) 571–576.
[20] F. Tai, F. Guo, M.T. Han, Z.D. Xia, Y.P. Lei, Y.W. Shi, Mater. Sci. Eng. A 527 (2010) 3335–3342.
[21] W.M. Xiao, Y.W. Shi, G.C. Xu, R. Ren, F. Guo, Z.D. Xia, Y.P. Lei, J. Alloys Compd. 472 (2009) 198–202.
[22] J. Shen, Y.C. Chan, J. Alloys Compd. 477 (2009) 552–559.
[23] L.C. Tsao, S.Y. Chang, Mater. Des. 31 (2010) 990–993.
[24] J.W. Yoon, S.W. Kim, S.B. Jung, J. Alloys Compd. 392 (2005) 247–252.
[25] J.W. Yoon, S.B. Jung, J. Alloys Compd. 458 (2008) 200–207.
[26] G.J. Zhang, Y.J. Sun, R.M. Niu, J. Sun, J.F. Wie, B.H. Zhao, L.X. Yang, Adv. Eng. Mater. 6 (12) (2004) 943–948.